

1. Terminal and non-terminal processing domains:

The idea of terminal domains suggests that we are limited by what our current physics can observe, measure and model, based on our technological tools and instruments.

Non-terminal domains would be those that are not directly accessible to our current senses or technology, but are still part of reality. In these domains, quantum phenomena or structures could exist that indirectly affect the visible universe.

2. Non-terminal processing in physics:

The concept of "processing" can be understood as the laws and dynamics that govern the evolution of the universe. In a non-terminal domain, the rules could be more general or different from the physical laws we know.

In this context, we could imagine that there are levels of existence or dimensions where current physical laws do not apply in the same way or are a "projection" of deeper, more abstract rules.

3. The KBC supervoid and the Hubble bubble:

The low-density region (the KBC supervoid) could offer an interesting framework to speculate on how these non-terminal domains might influence the observable universe.

If our galaxy is in a less dense region, that implies that gravitational interactions and other properties of space-time could be different from those in more dense regions. This opens questions about whether this bubble is a reflection of physical processes operating from a non-terminal domain.

4. Limited instruments:

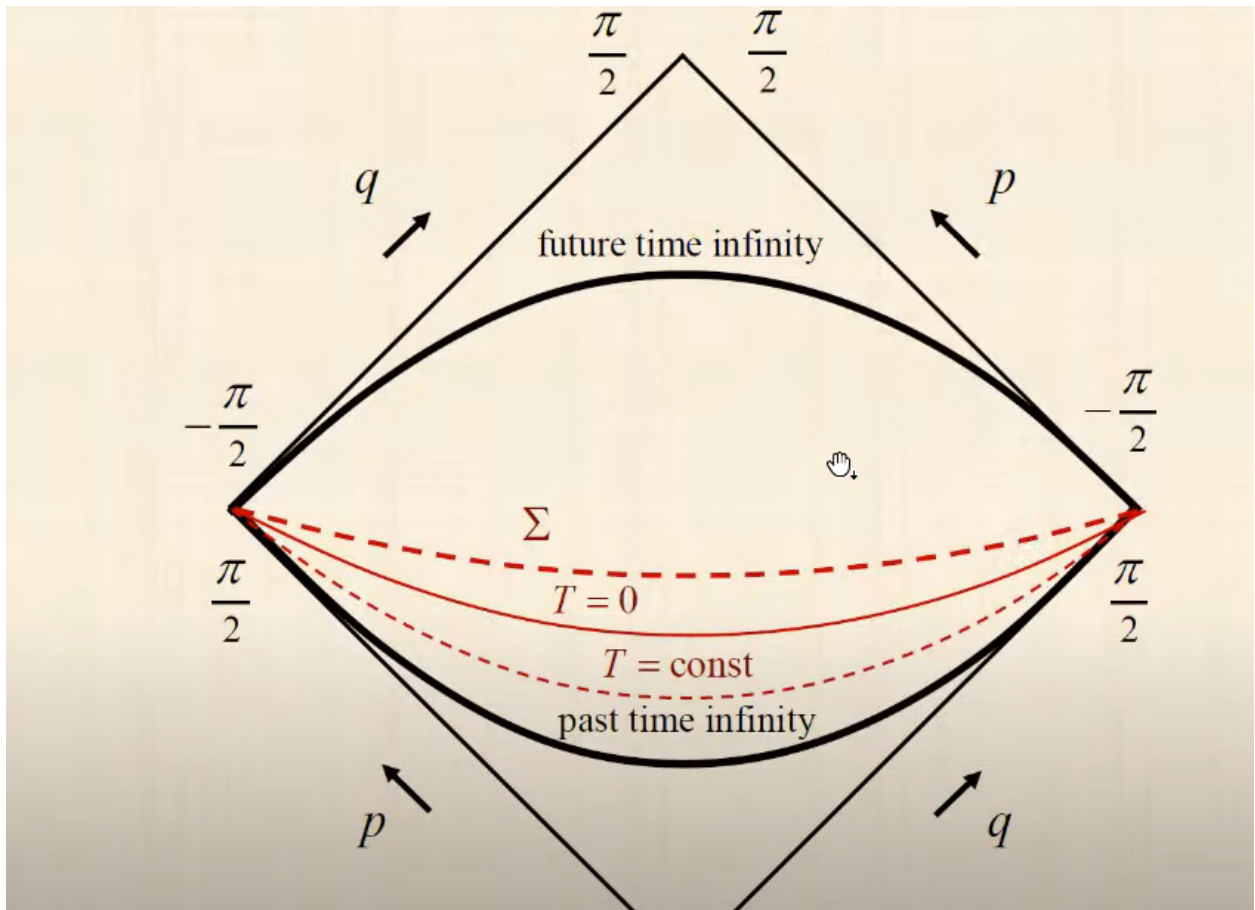
As you point out, our ability to explore these phenomena is restricted by current technology and theories. Current instruments are designed to operate within the framework of the terminal domain (observable dimensions and accessible energies).

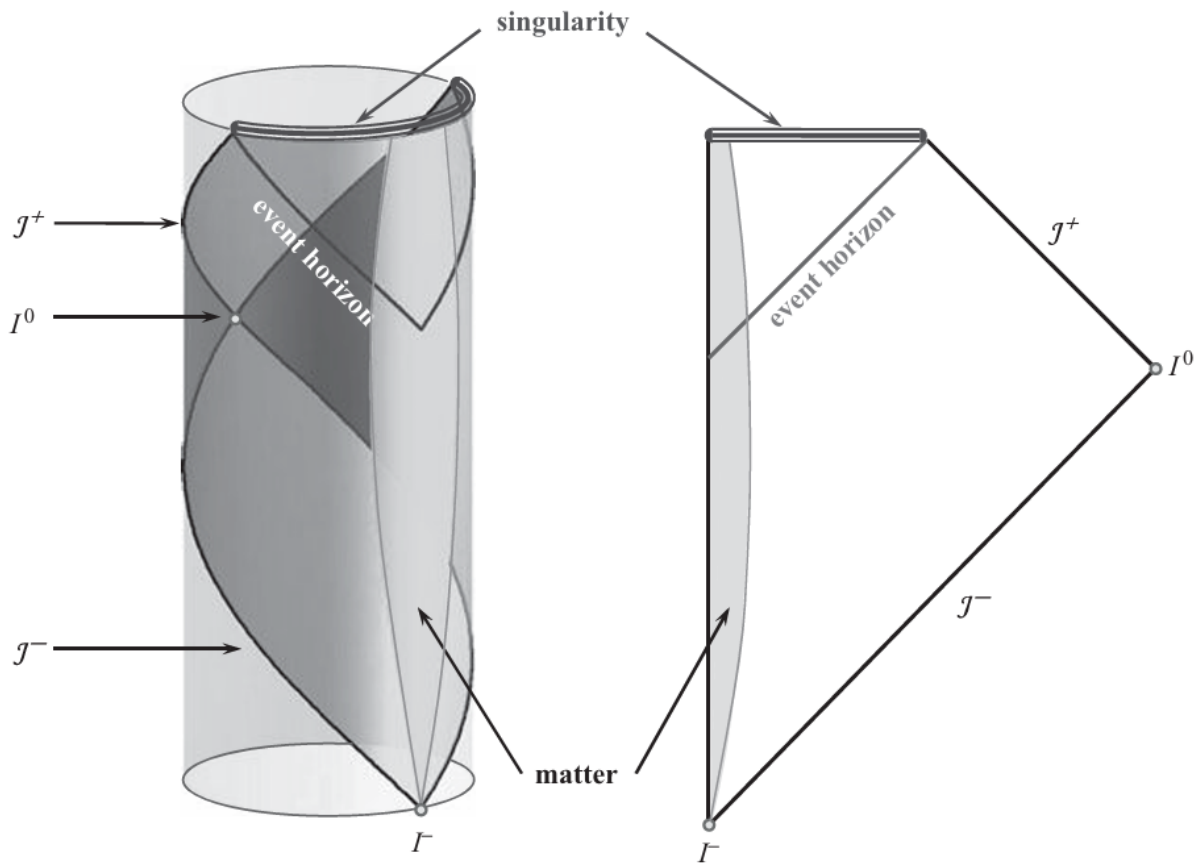
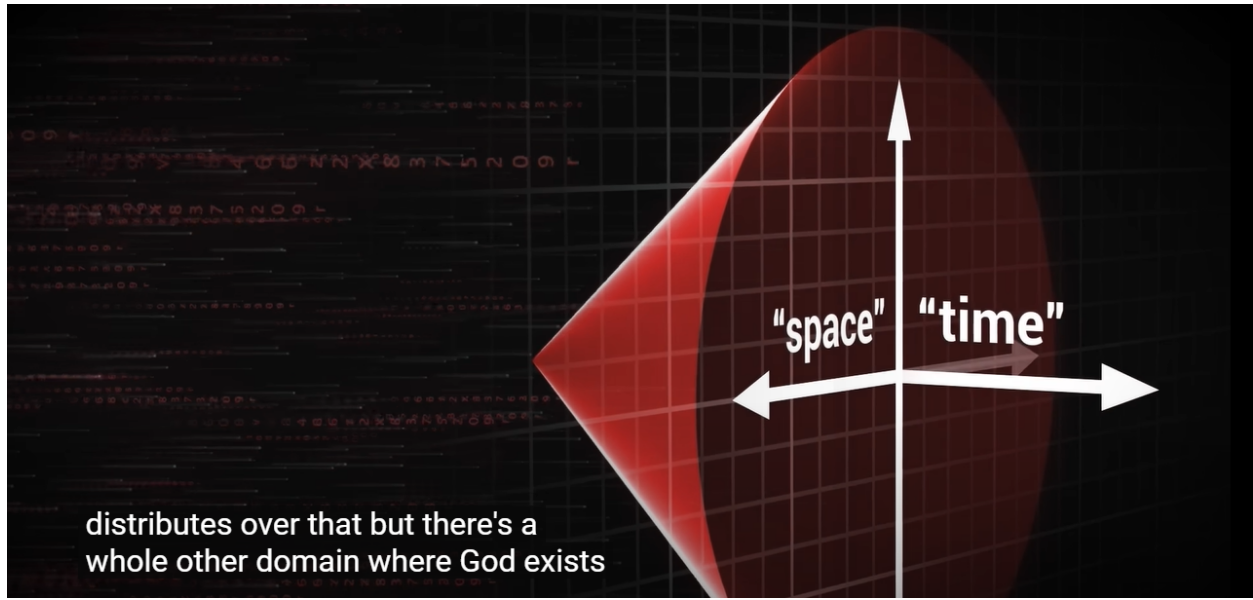
If there are phenomena associated with non-terminal domains, we would need a new generation of instruments or theoretical approaches that connect these realities.

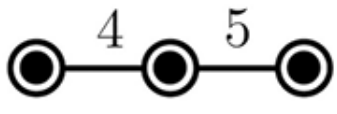
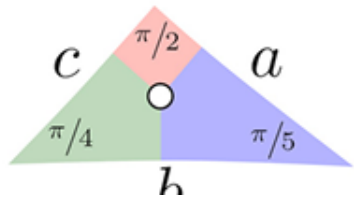
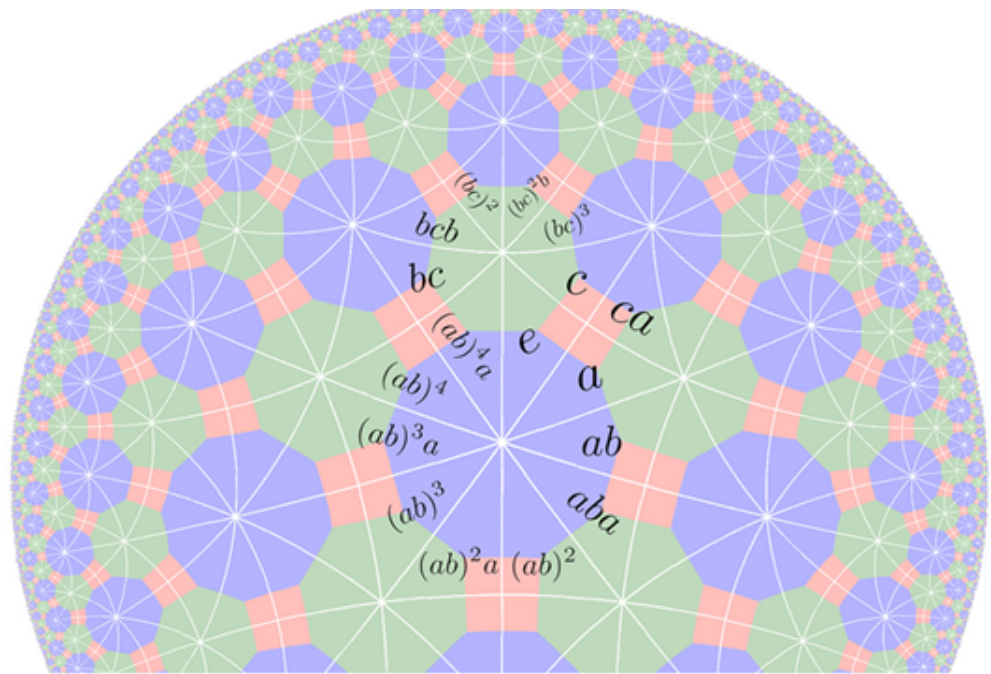
5. Connection with quantum physics and processing at invisible scales:

Quantum physics already shows signs of phenomena that have no clear analogy in the macroscopic world, such as entanglement or wave-particle duality.

If we expand on these ideas, we might think of scales or dimensions where quantum interactions have properties that are not only invisible, but operate in domains that are not directly connected to the "terminals" of the observable universe.

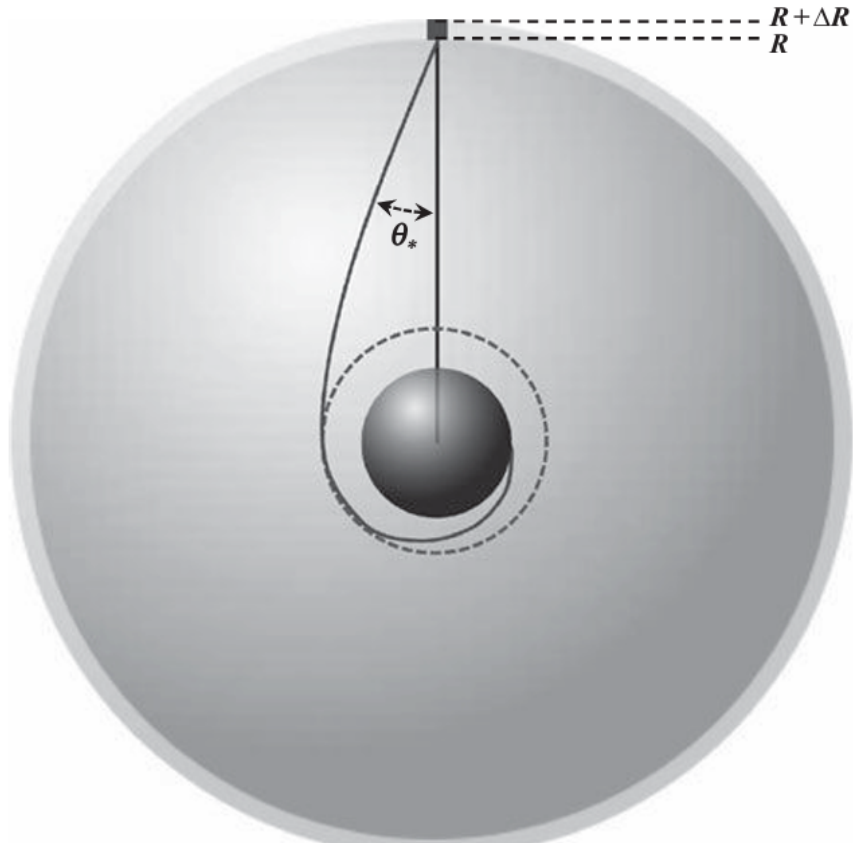






Since for large R the angle θ_* is very small one has

$$\int_0^{\theta_*} d\theta \sin \theta \approx (\theta_*)^2/2 = \frac{27}{8} \left(\frac{r_s}{R}\right)^2.$$



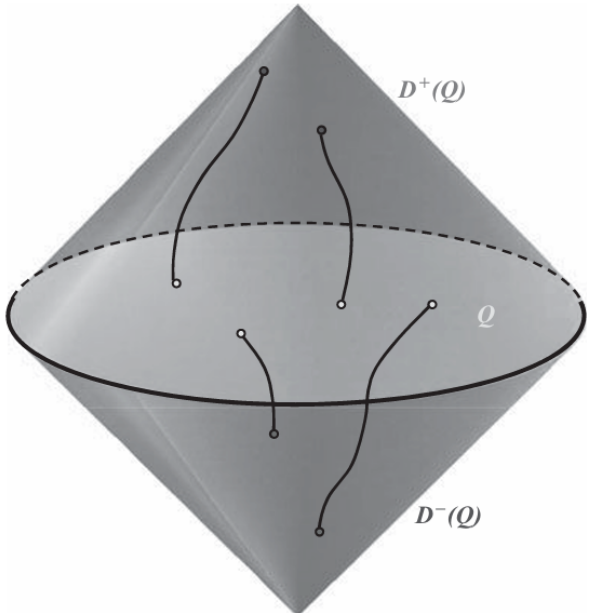


Fig. 3.6 Illustration of the future and past Cauchy domains for the set Q .

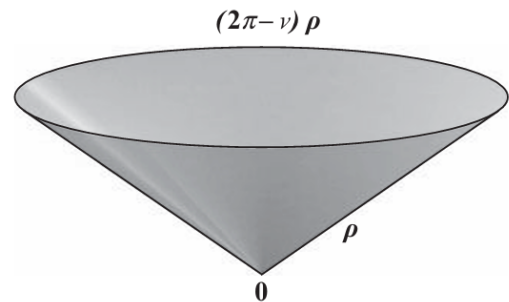


Fig. 2.8 Geometry of the $(\tau-\rho)$ -sector of the space Eq. (2.6.6). The figure shows the embedding diagram for this sector in the 3D flat pace for the positive angle deficit ν . For $\nu \neq 0$ the surface has a *conical singularity* at $\rho = 0$.

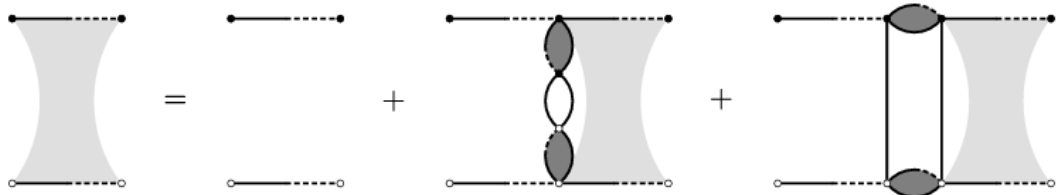


Figure 4: A diagrammatic representation of the Bethe-Salpeter equation that sums the leading order corrections to the averaged correlator (2.2). The lines denote the resummed tadpole diagrams from Fig. 2. The dark gray loops denote the resummed bubble chain diagrams from Fig. 3. The light gray block denotes the resummed four-point correlator (2.2).

3. Finding a starting point on the center path using self-dual embedding. Path-following primary dual IPMs find the optimal point by starting at a central point with $v>0$ and following the central path to a very small value of v , which is considered a good approximation of the optimal point. For a given SOCP, finding a starting point on the central path is non-trivial and can often be as difficult as solving the SOCP itself. One solution to this problem is homogeneous self-dual embedding [51,52], where a slightly larger self-dual SOCP is formed with the properties that (i) the optimal point for the original SOCP can be determined from the optimal point for the Autodual SOCP and (ii) Autodual SOCP has a trivial center point that can be used to initialize the IPM. To do this, we introduce new scalar variables τ , θ and κ , which are used to give more flexibility to the constraints. Previously, we required $Ax = b$. In the broader program, we relax this constraint to read $Ax = b\tau - (b - Ae)\theta$, so that the original constraint is recovered when $\tau = 1$ and $\theta = 0$ but $x = e$ is a trivial solution when $\tau = 1$ and $\theta = 1$. Similarly, we relax the constraint $A^\top y + s = 0$ to $A^\top y + s = c\tau - (c - e)\theta$, which has the trivial solution $y = 0$, $s = e$ when $\tau = 0 = 1$. We complement them with two additional linear constraints to form the program $\min_{(x,y,\tau,\theta,s,\kappa)} (x^\top y + s) \tau + (c^\top x + s) \theta$ such that (13) $\begin{cases} A^\top x = b \\ A^\top y + s = c \\ x \in Q \\ \tau, \theta, s \geq 0 \\ \tau + \kappa = 1 \end{cases}$, where $b = b - Ae$, $c = c - e$, $r = e^\top e$ is the number of cones in the original SOCP. While Eq. (13) does not have exactly the form given in Eq. (5), we can still consider it as a primary SOCP. Since the block matrix in Eq. (13) is asymmetric and the coefficients of the objective function are equal to the right side of the equality constraints, when we compute the dual program [cf. Eq. (6)], we obtain an equivalent program; We conclude that Eq. (13) is self-dual [51]. Therefore, when applying the path that follows the primary dual MPIs to equation (13), we only need to keep track of the primary variables, i.e., x , y , τ , θ , s , κ . Given the sum of τ and κ , they are effectively an additional pair of primaries. -dual variables, the duality gap was defined [cf. (7)] as $\mu(x, \tau, s, \kappa) := \frac{1}{r+1} (x^\top s + \kappa \tau)$. (14) Note that if the point $(x, y, \tau, \theta, s, \kappa)$ is feasible, that is, if it satisfies the four linear constraints in Eq. (13), then we have the identity

$$\mu(x, \tau, s, \kappa) = -x^\top A^\top y + x^\top c\tau - x^\top c\theta + \kappa \tau = -b^\top y\tau + b^\top y\theta + x^\top c\tau - x^\top c\theta + \kappa \tau = -b^\top y\theta - x^\top c\theta + z^\top \theta = 0$$

6.5.7 Babbage difference engine emulation circuit

The Babbage difference engine is a mechanical digital computation device designed to tabulate a polynomial function. It was proposed by Charles Babbage, an English mathematician, in the nineteenth century. The engine is based on Newton's method of differences and avoids the need for multiplication. For example, consider a second-order polynomial $f(n) = 2n^2 + 3n + 5$. We can find the difference between $f(n)$ and $f(n - 1)$:

$$f(n) - f(n - 1) = 4n + 1$$

Assume that n is an integer and $n \geq 0$. The $f(n)$ can be defined recursively as

$$f(n) = \begin{cases} 5 & \text{if } n = 0 \\ f(n - 1) + 4n + 1 & \text{if } n > 0 \end{cases}$$

This process can be repeated for the $4n + 1$ expression. Let $g(n) = 4n + 1$. We can find the difference between $g(n)$ and $g(n - 1)$:

$$g(n) - g(n - 1) = 4$$

The $g(n)$ can be defined recursively as

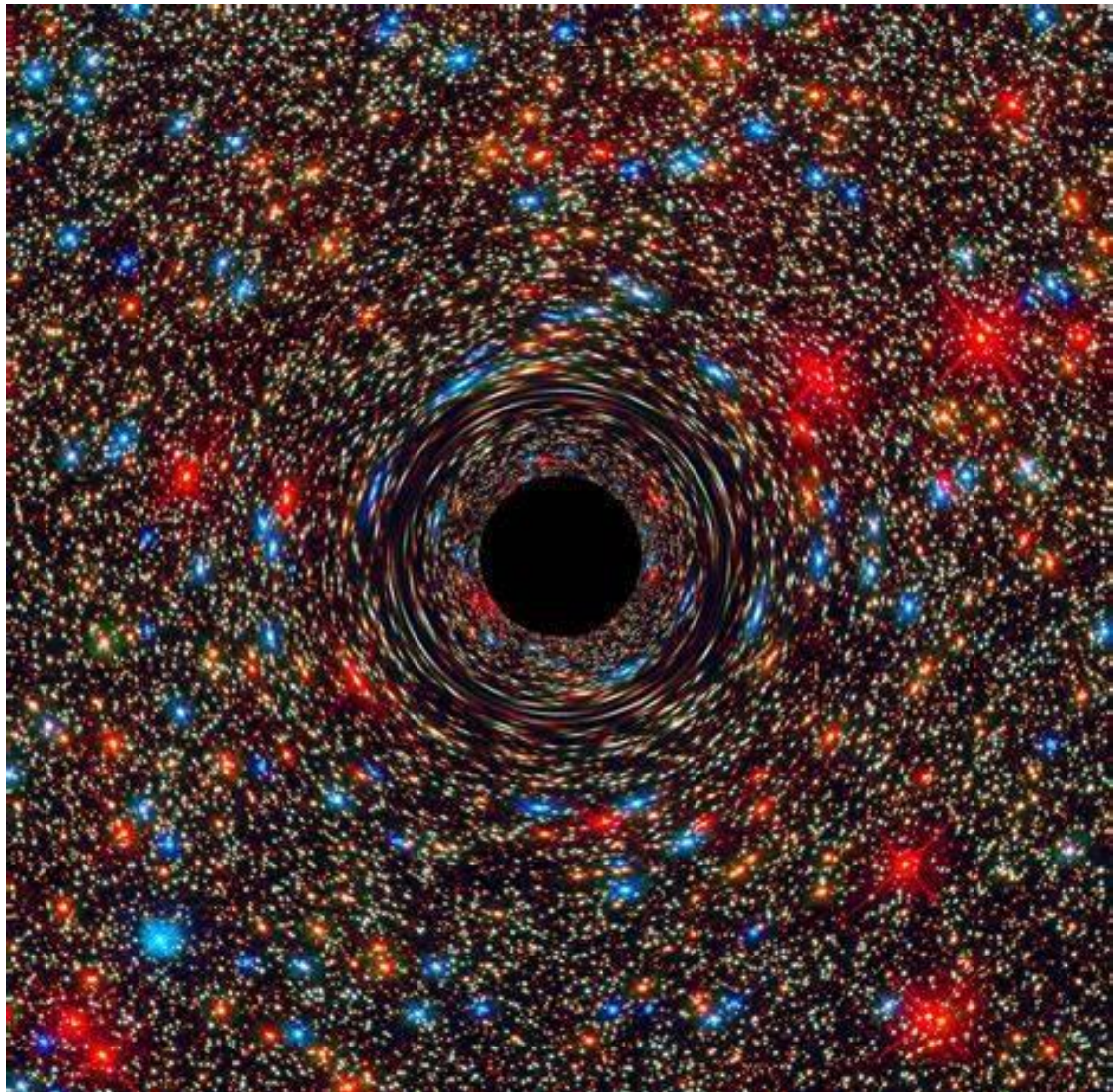
$$g(n) = \begin{cases} 5 & \text{if } n = 1 \\ g(n - 1) + 4 & \text{if } n > 1 \end{cases}$$

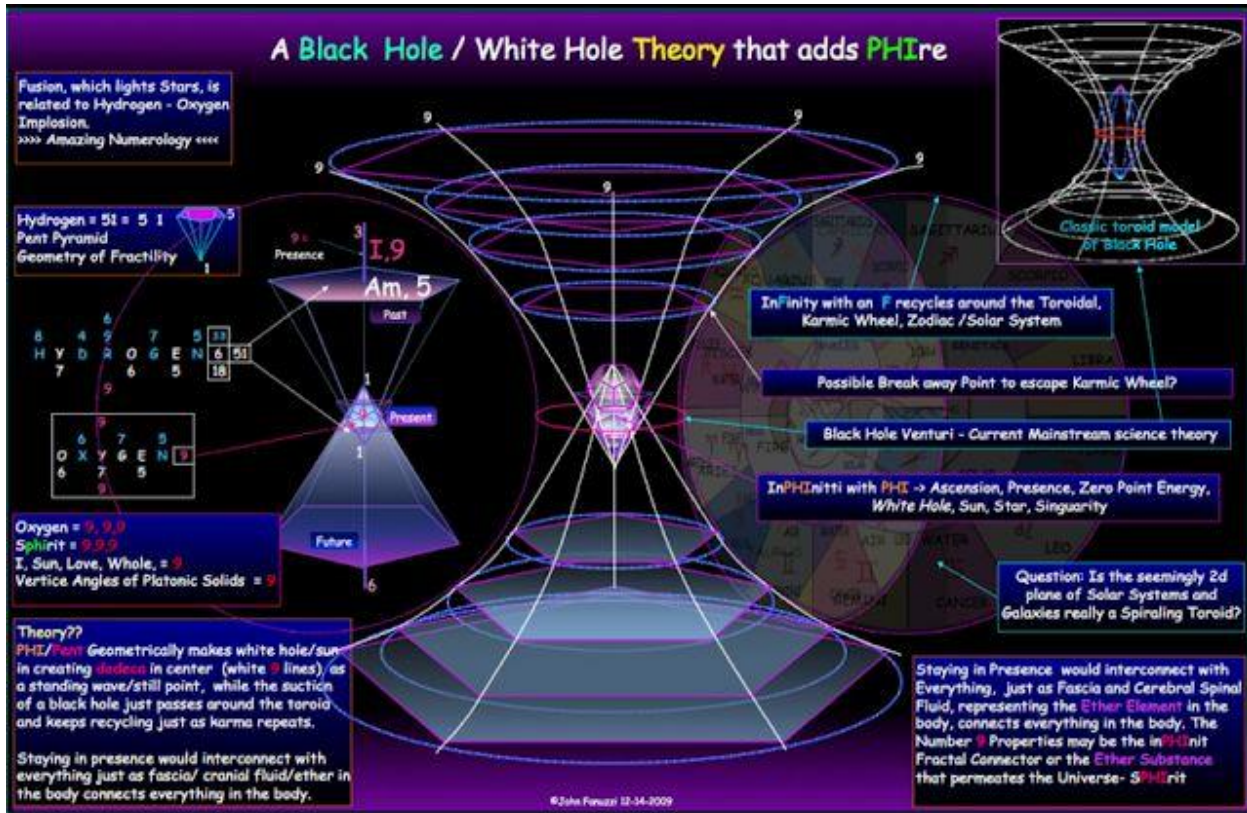
and $f(n)$ can be rewritten as

$$f(n) = \begin{cases} 5 & \text{if } n = 0 \\ f(n - 1) + g(n) & \text{if } n > 0 \end{cases}$$

Note that only additions are involved in the recursive definitions of $f(n)$ and $g(n)$.

Based on the definition of the last two recursive equations, we can derive an algorithm to compute $f(n)$. Two temporary registers are needed to keep track of the most recently calculated $f(n)$ and $g(n)$, and two additions are needed to update $f(n)$ and $g(n)$. Assume





Input: SOCP instance $(A, \mathbf{b}, \mathbf{c})$, list of cone sizes (N_1, \dots, N_r) and tolerance ϵ
Output: Vector \mathbf{x} that optimizes objective function (eq. (5)) to precision ϵ

/* For portfolio optimization, A , \mathbf{b} , \mathbf{c} are given in eq. (10). First n entries of \mathbf{x} give optimal stock weights. */

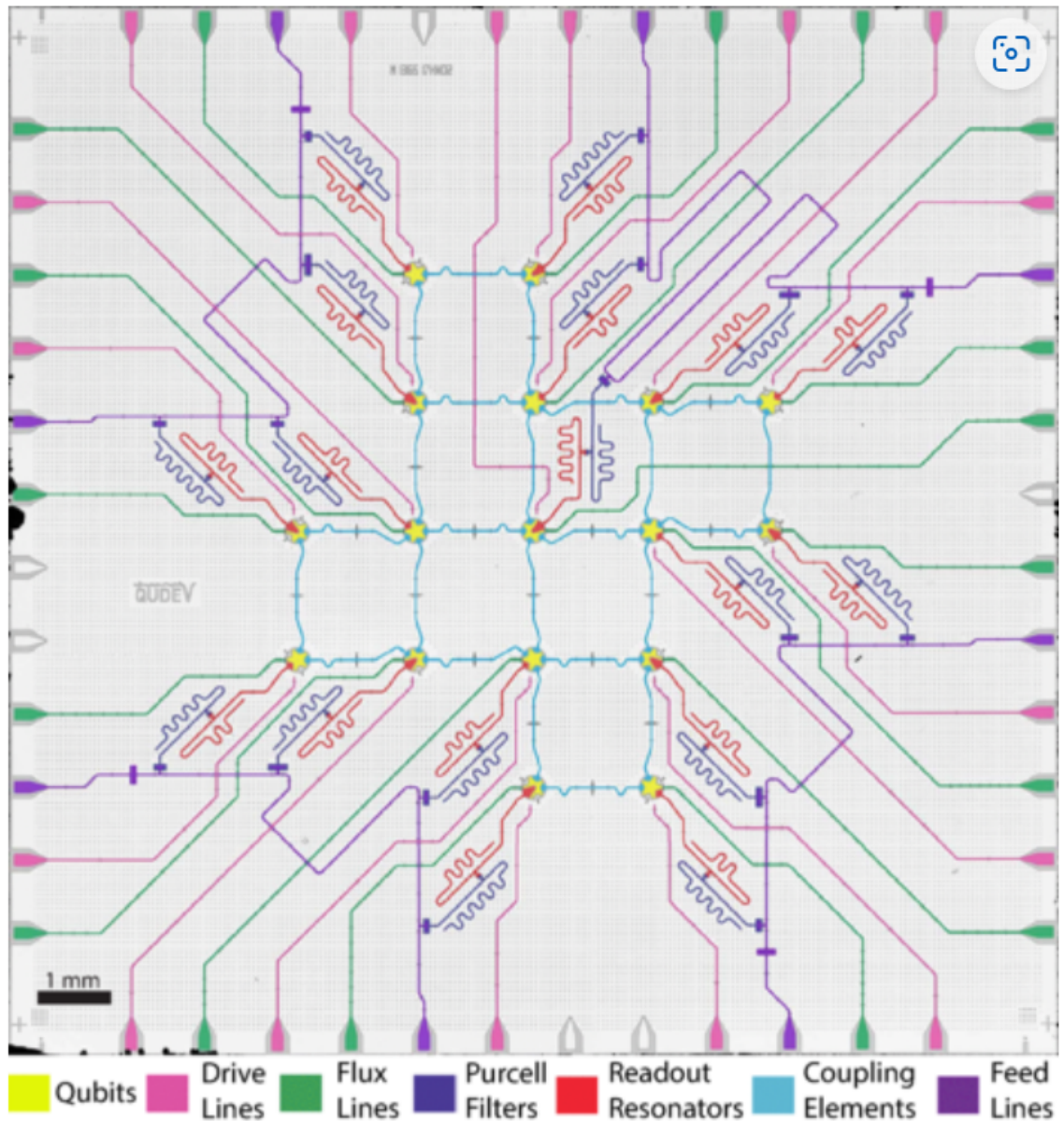
```

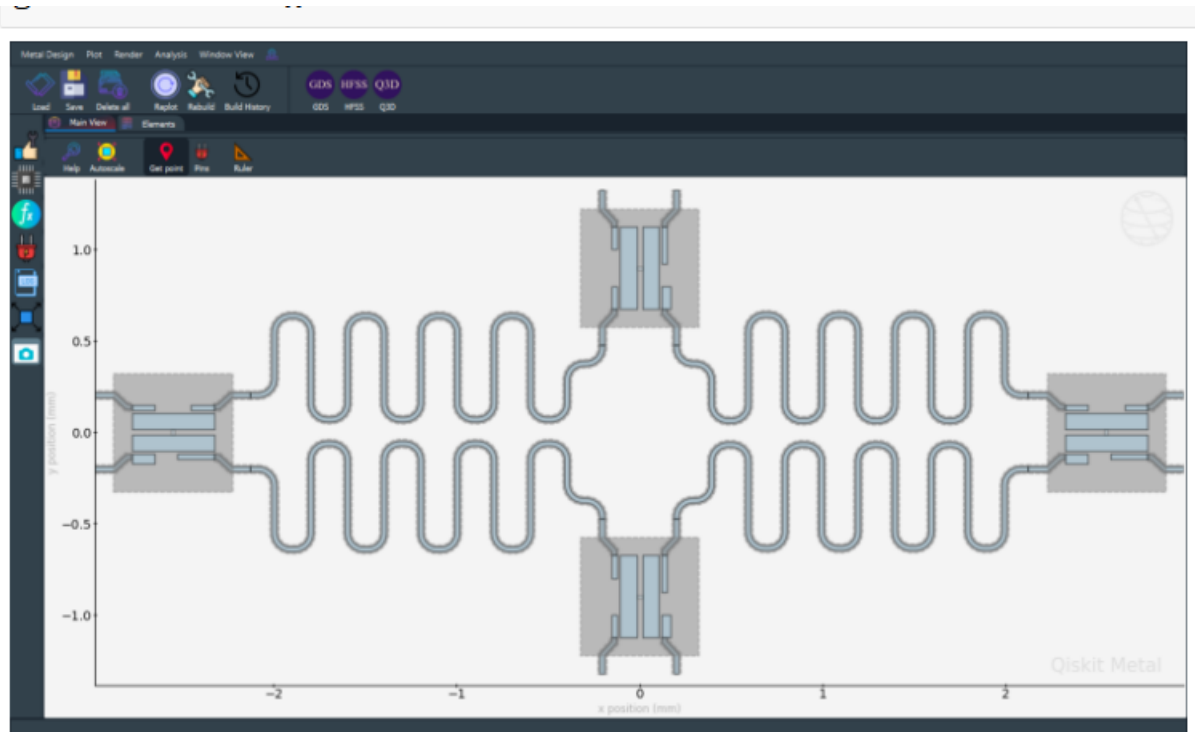
1  $(\mathbf{x}; \mathbf{y}; \tau; \theta; \mathbf{s}; \boldsymbol{\alpha}) \leftarrow (\mathbf{e}; \mathbf{0}; 1; 1; \mathbf{e}; 1)$  /* initialize on central path */
2  $\mu \leftarrow 1, \sigma \leftarrow 1 - \frac{1}{20\sqrt{2}} \frac{1}{\sqrt{\pi}}, \gamma \leftarrow 1/10$  /* set parameters */
3 while  $\mu \geq \epsilon$ : /* Follow central path until duality gap less than  $\epsilon$  */
4    $G \leftarrow \begin{pmatrix} 0 & A^\top & -\mathbf{c} & \bar{\mathbf{c}} & I & 0 \\ -A & 0 & \mathbf{b} & -\bar{\mathbf{b}} & 0 & 0 \\ \mathbf{c}^\top & -\bar{\mathbf{b}}^\top & 0 & -\bar{z} & 0 & 1 \\ -\bar{\mathbf{c}}^\top & \bar{\mathbf{b}}^\top & \bar{z} & 0 & 0 & 0 \\ S & 0 & 0 & X & 0 & 0 \\ 0 & 0 & \boldsymbol{\alpha} & 0 & 0 & \tau \end{pmatrix}$  /* from eqs. (19) and (22) */
5    $\mathbf{h} \leftarrow \begin{pmatrix} -A^\top \mathbf{y} + c\tau - \bar{c}\theta - \mathbf{s} \\ Ax - b\tau + \bar{b}\theta \\ -c^\top \mathbf{x} + b^\top \mathbf{y} + \bar{z}\theta \\ \bar{c}^\top \mathbf{x} - \bar{b}^\top \mathbf{y} - \bar{z}\tau \\ \sigma\mu e - \tilde{X}\tilde{S}\mathbf{e} \\ \sigma\mu - \boldsymbol{\alpha}\tau \end{pmatrix}$  /* mat.-vec. mult. performed classically */
6   for  $j = 1, \dots, L$ : /* preconditioning via row normalization */
7      $g \leftarrow \sqrt{\sum_k |G_{jk}|^2}$  /* norm of  $j$ th row of  $G$  */
8      $h_j \leftarrow h_j/g$ 
9     for  $k = 1, \dots, L$ :
0        $| G_{jk} \leftarrow G_{jk}/g$ 
1   Classically compute  $L^2$  angles and gate decompositions necessary to perform block-encoding of  $G$  and state-preparation of  $|\mathbf{h}\rangle$  (see Ref. [33])
2    $\xi \leftarrow 1$ 
3   repeat /* try smaller and smaller  $\xi$  until central path is found */
4      $\xi \leftarrow \xi/2$ 
5      $(\Delta\mathbf{x}; \Delta\mathbf{y}; \Delta\tau; \Delta\theta; \Delta\mathbf{s}; \Delta\boldsymbol{\alpha}) \leftarrow \text{ApprSolve}(G, \mathbf{h}, \xi)$ 
6     (step length)  $\leftarrow \frac{\mu(\sigma-1)(r+1)}{(\Delta\mathbf{x})^\top \mathbf{s} + (\Delta\mathbf{s})^\top \mathbf{x} + (\Delta\boldsymbol{\alpha})^\top \tau + (\Delta\tau)^\top \boldsymbol{\alpha}}$ 
7      $(\mathbf{x}'; \mathbf{y}'; \tau'; \theta'; \mathbf{s}'; \boldsymbol{\alpha}') \leftarrow (\mathbf{x}; \mathbf{y}; \tau; \theta; \mathbf{s}; \boldsymbol{\alpha}) + (\text{step length}) \cdot (\Delta\mathbf{x}; \Delta\mathbf{y}; \Delta\tau; \Delta\theta; \Delta\mathbf{s}; \Delta\boldsymbol{\alpha})$ 
8   until  $(\mathbf{x}'; \mathbf{y}'; \tau'; \theta'; \mathbf{s}'; \boldsymbol{\alpha}') \in \mathcal{N}(\gamma)$ 
9    $(\mathbf{x}; \mathbf{y}; \tau; \theta; \mathbf{s}; \boldsymbol{\alpha}) \leftarrow (\mathbf{x}'; \mathbf{y}'; \tau'; \theta'; \mathbf{s}'; \boldsymbol{\alpha}')$ 
0    $\mu \leftarrow \sigma\mu$ 
1   return  $\mathbf{x}/\tau$ 

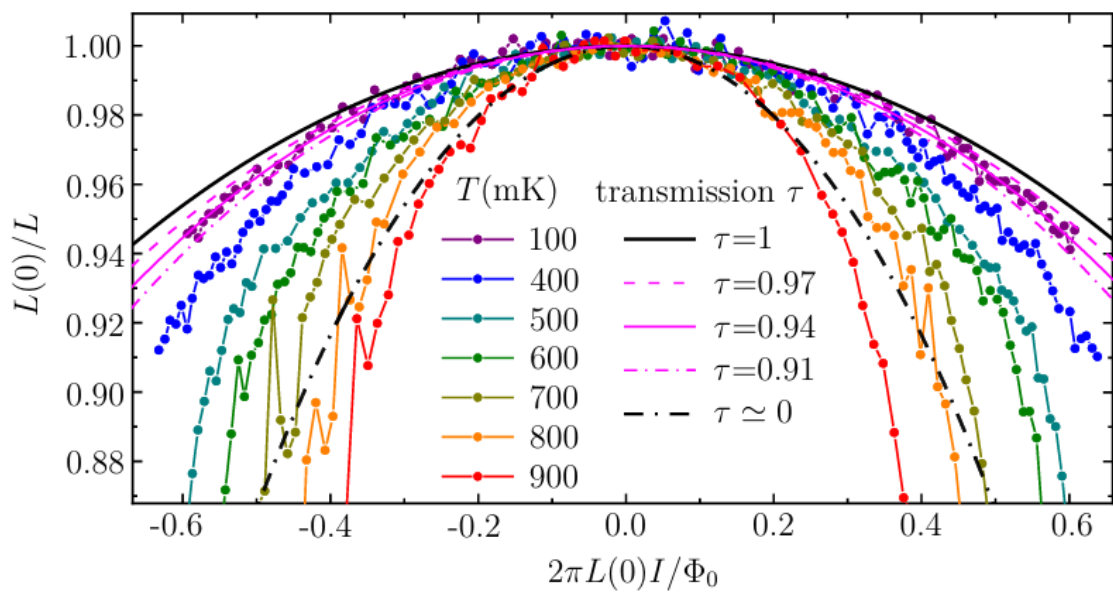
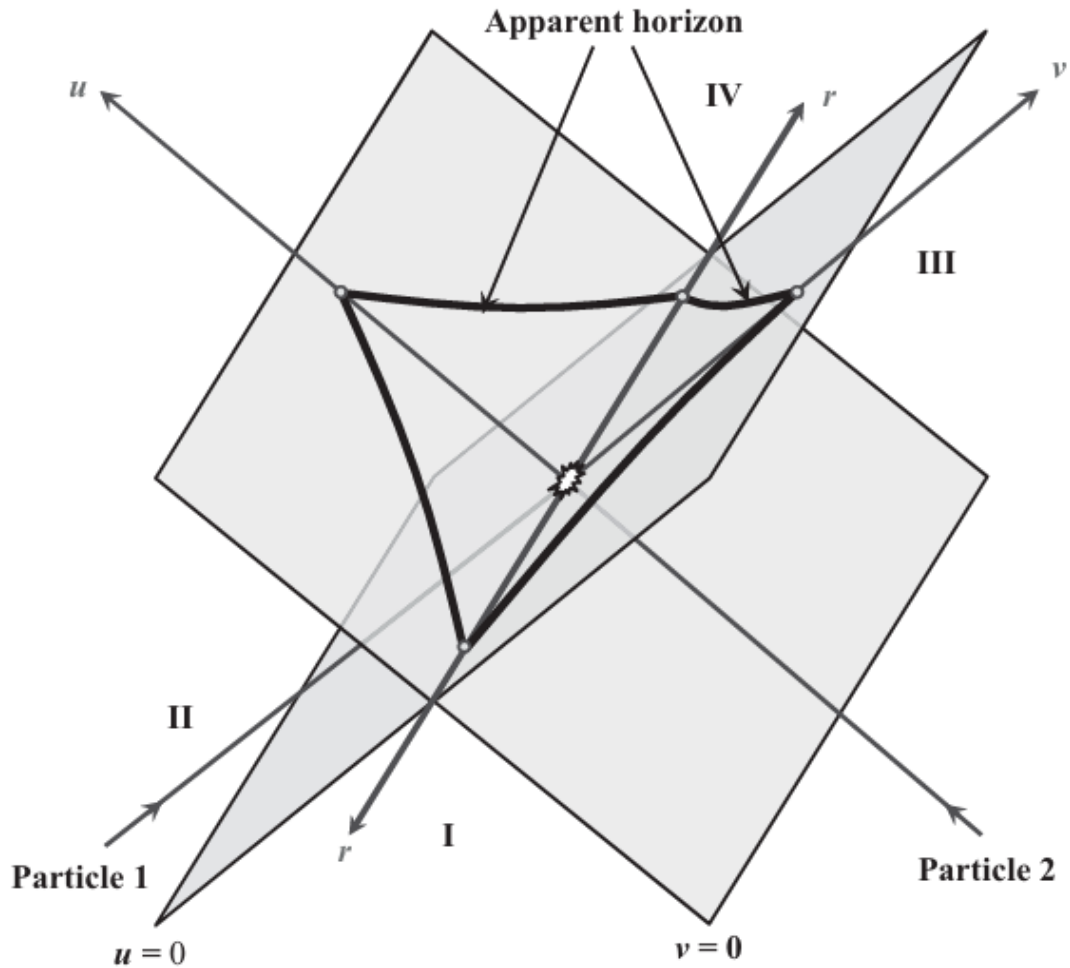
2 def ApprSolve( $G, \mathbf{h}, \xi$ ):
3    $L \leftarrow 2N + K + 3$ 
4    $\delta \leftarrow 0.1$ 
5    $\varepsilon \leftarrow 0.9\xi$ 
6    $k \leftarrow 57.5L \ln(6L/\delta)/(\varepsilon^2(1 - \varepsilon^2/4))$ 
7   Run tomography as described in section IV D using  $k$  applications and  $k$  controlled-applications of the QLSS algorithm on the system  $(G, \mathbf{h})$ 
8   return Vector  $\tilde{\mathbf{v}}'$  for which  $\|\tilde{\mathbf{v}}'\| = 1$  and  $\|\tilde{\mathbf{v}}' - \mathbf{v}\| \leq \xi$  with probability at least  $1 - \delta$ , where  $\mathbf{v} \propto G^{-1}\mathbf{h}$ 

```

FIG. 8.







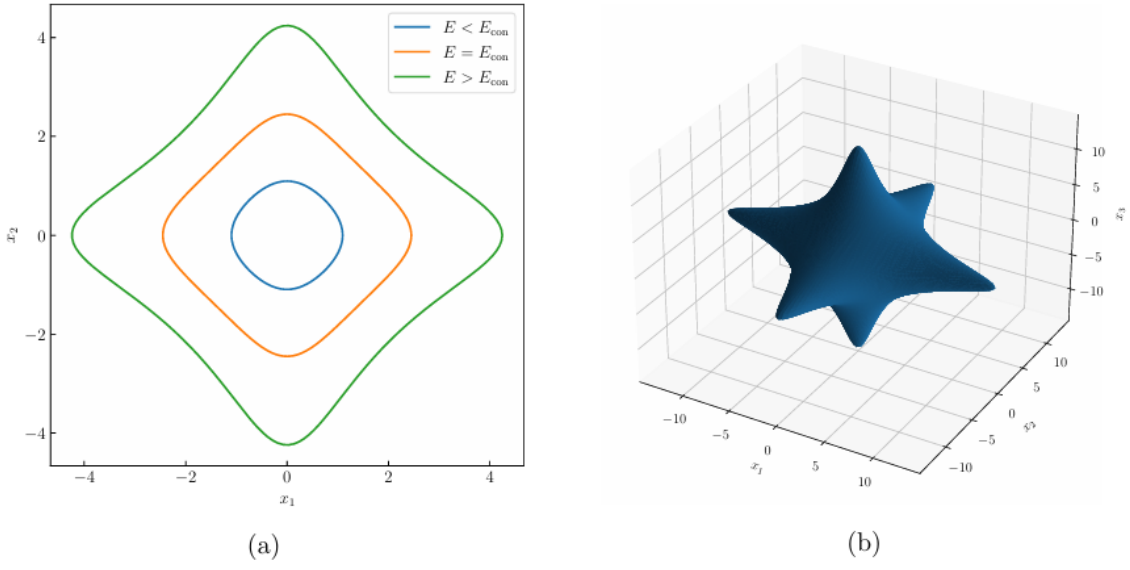


Figure 8: (a) constant (potential) energy curve for $N = 2$ and $E < E_{\text{con}}$ (blue line), $E = E_{\text{con}}$ (orange line), $E > E_{\text{con}}$ (green line). (b) constant energy surface for $N = 3$ and $E \gg E_{\text{con}}$. All the quantities are dimensionless (cf. (3.17)–(3.18)).

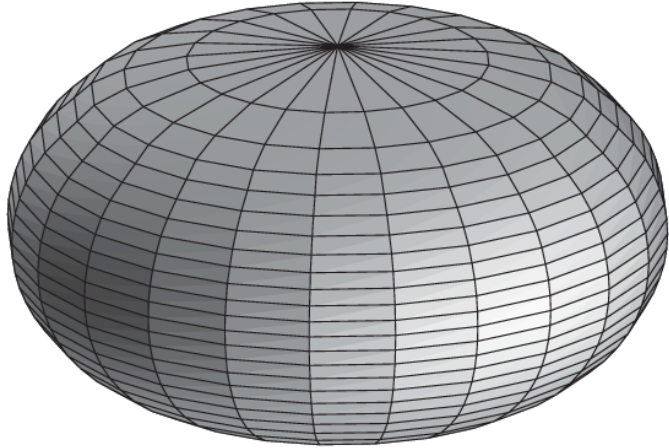


Fig. 8.2 The embedding diagram for a two-dimensional section of the event horizon of the Kerr black hole. The diagram is constructed for the critical value $a/M = \sqrt{3}/2$ of the rotation parameter so that the Gaussian curvature vanishes at the poles.

The length of the equatorial circle $\theta = \frac{\pi}{2}$ for the metric dS^2 is

$$L_l = \frac{2\pi}{\sqrt{1 - \beta^2}}. \quad (8.2.48)$$

$$dS^2 = [1 + (d\rho/dZ)^2] dZ^2 + \rho^2 d\phi^2.$$

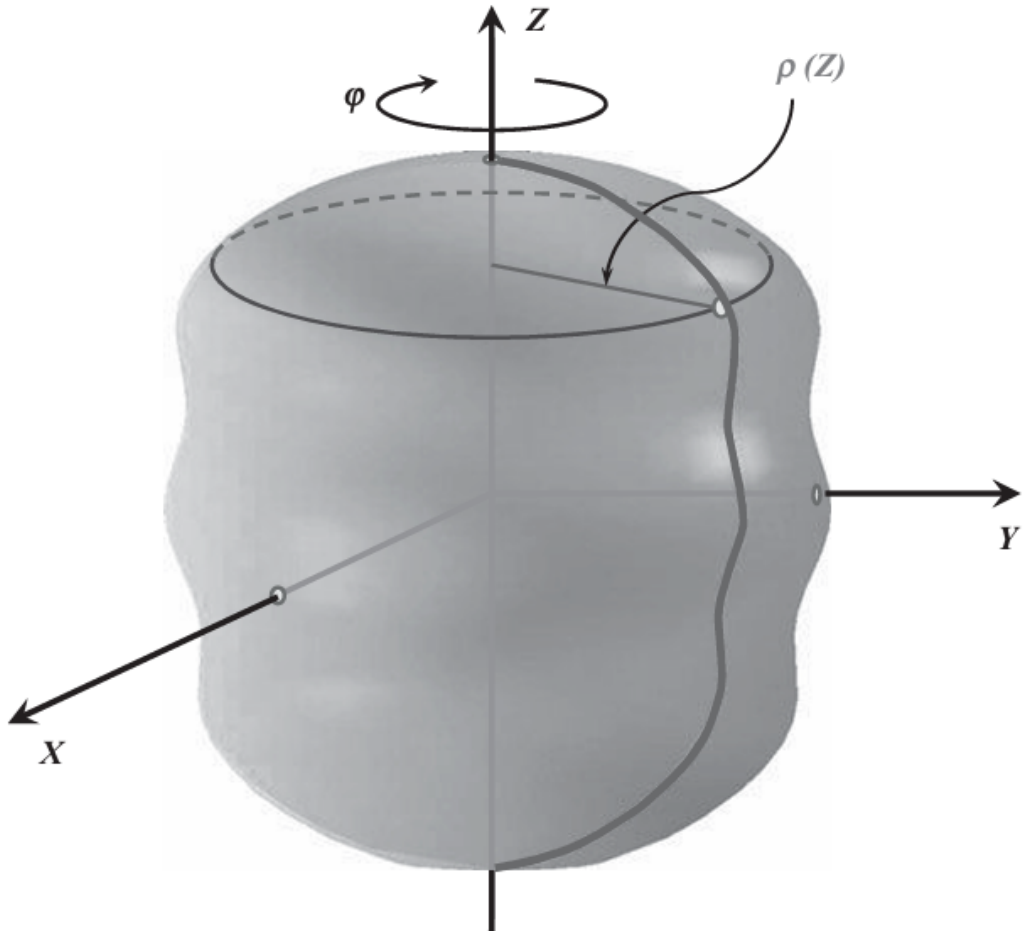
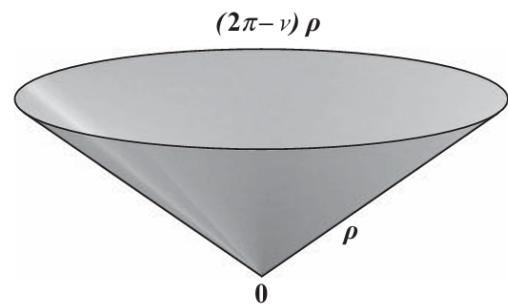


Fig. 8.1 A surface of revolution.

Fig. 2.8 Geometry of the $(\tau-\rho)$ -sector of the space Eq. (2.6.6). The figure shows the embedding diagram for this sector in the 3D flat space for the positive angle deficit ν . For $\nu \neq 0$ the surface has a *conical singularity* at $\rho = 0$.



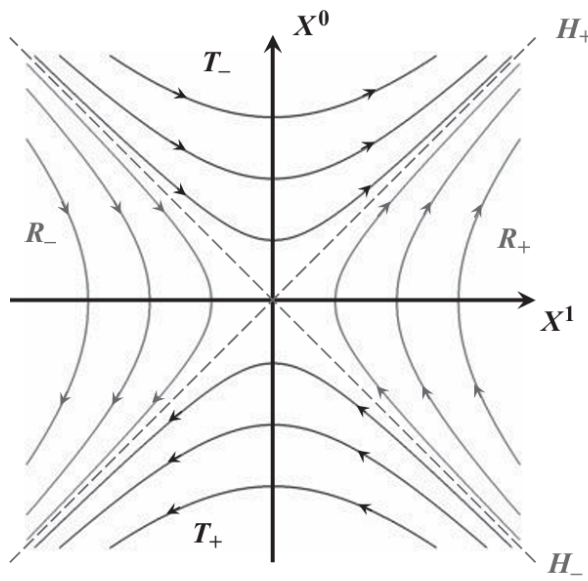


Fig. 2.7 Integral lines of the boost Killing vector in the $(X^0 - X^1)$ -plane. These lines are future directed in R_+ and are past directed in R_- . In T_{\pm} they are space-like. These integral lines are tangent to the horizons H_{\pm} and coincide there with the horizon generators.

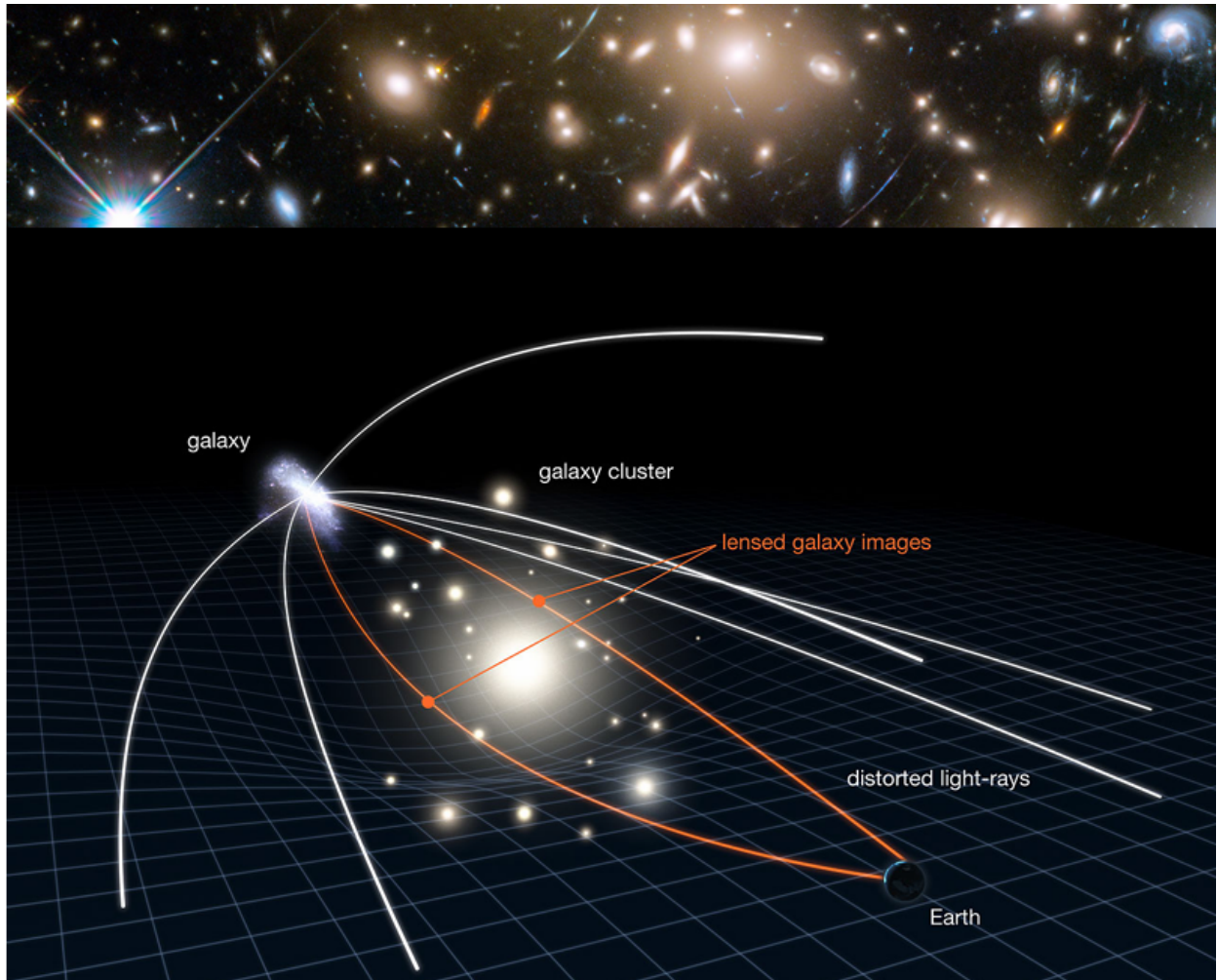
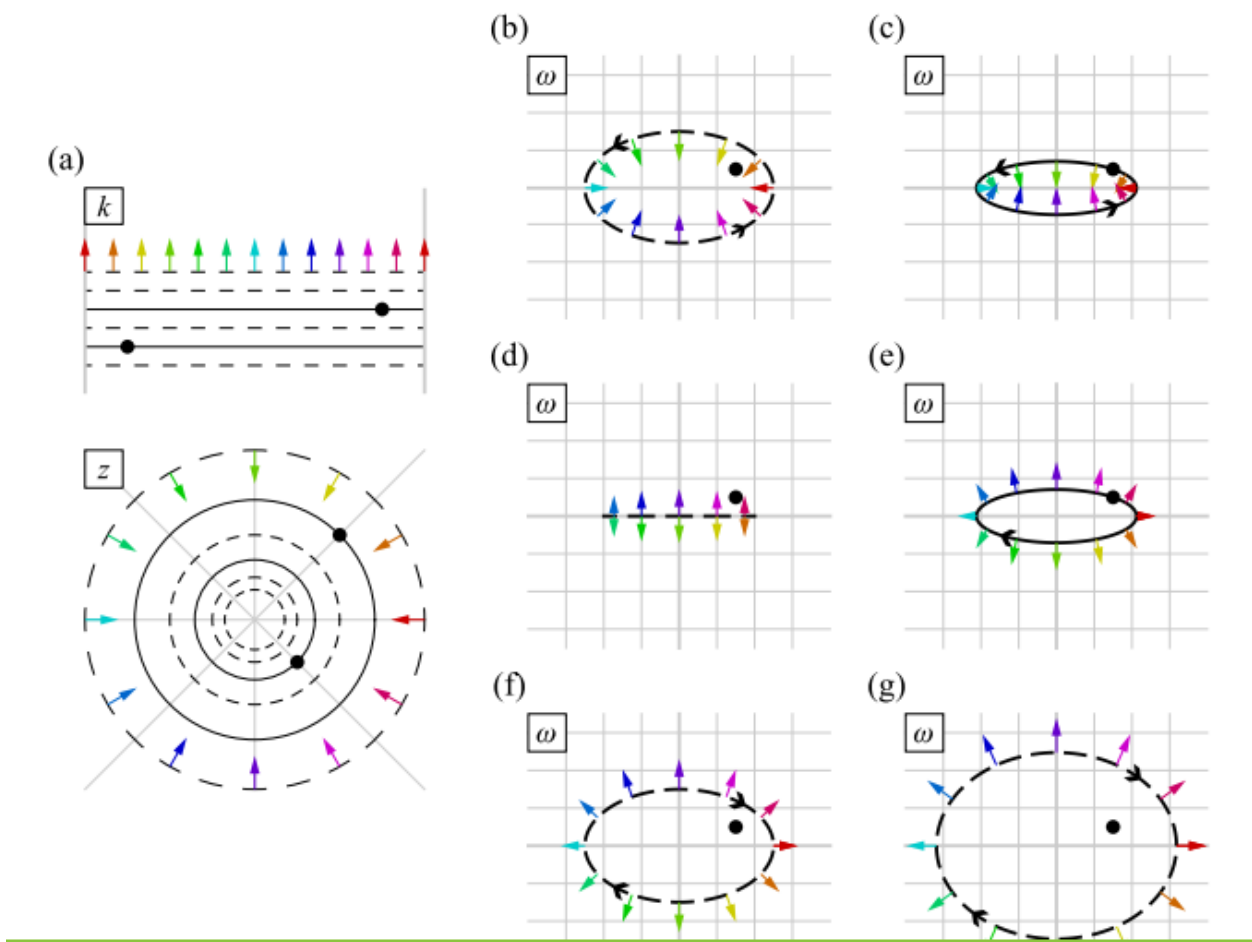
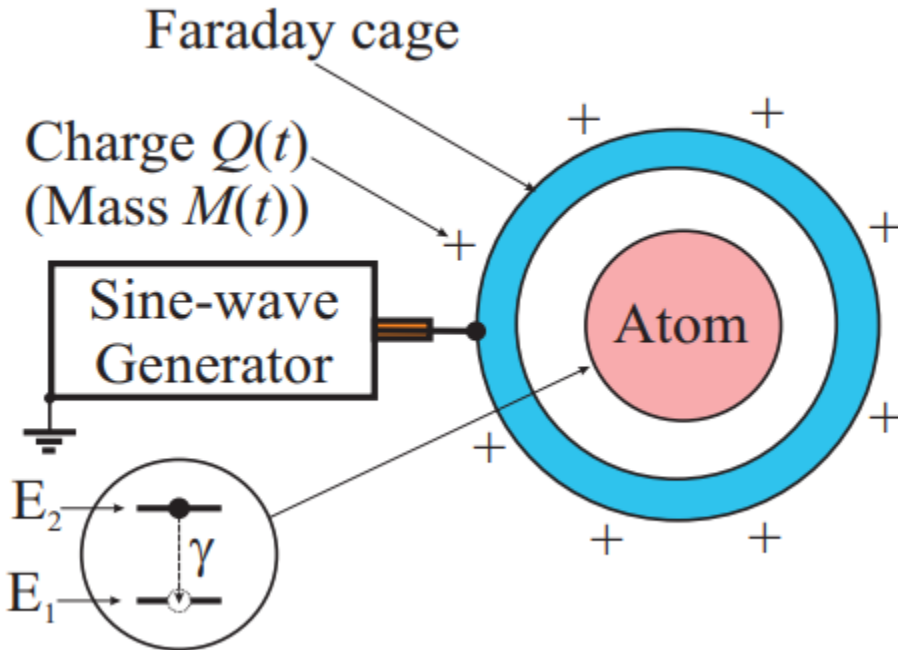
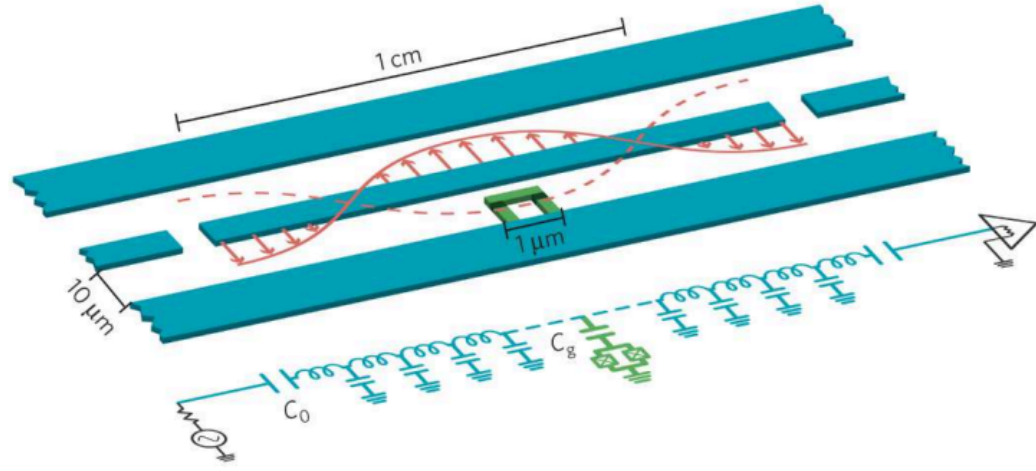


Figure 15





4. Iteration of the IPM Each iteration of the IPM takes as input an intermediate point $(x; y; \tau; \theta; s; \kappa)$ that is feasible (or in some formulas, almost feasible), has a duality gap $(x^\top s + \kappa\tau)/(r+1)$ equal to μ , and is close to the central path with parameter $v=\mu$. The output of the iteration is a new intermediate point $(x^+ \text{ feasible})$ and is close to the central path, with a small value of v . Therefore, iterate many sometimes leads to a solution with a duality gap arbitrarily close to zero. An additional input is the step size, governed by a parameter $\sigma < 1$. The IPM iteration aims to bring the next intermediate point to the central path with the parameter $v=\sigma\mu$. This is achieved by taking a step using Newton's method, where the vector $(x; y; \tau; \theta; s; \kappa)$ is uniquely determined by solving a linear system of equations called Newton's system. The first part of Newton's system are the conditions that must be met for the new point to be feasible, given in the following system of $N+K+2$ linear equations:

$$\begin{pmatrix} 0 & A^\top & -c^\top & -A & 0 & b^\top & -b & c^\top & -b^\top & 0 & -z^\top & -c^\top & -b^\top & -z^\top \end{pmatrix} = 0$$

$0 \leq \|J\| \leq \|Ax - b\tau + b\theta - c^T x + b^T y + z\theta - c^T x - b^T y - z\tau\|$. (19) Note that if the point is already feasible, the right side is equal to zero. The second part of the Newton system is the linearized conditions for reaching the central path point with a duality gap $\sigma\mu$. That is, we look for $(x + \bar{x})^T(s + \bar{s}) = \sigma\mu e$ and $(\kappa + \bar{\kappa})(\tau + \bar{\tau}) = \sigma\mu$. Ignoring the second-order terms (i.e., the terms $O(x^T s)$ and $O(\kappa \tau)$), these become $x^T s + \bar{x}^T \bar{s} = \sigma\mu e - x^T \bar{s}$, $\kappa \tau + \bar{\kappa} \bar{\tau} = \sigma\mu - \kappa \bar{\tau}$. (20) The above expression can be rewritten as a matrix equation by first defining the arrowhead matrix U for a vector $u = (u_0; u) \in Q$ as $U = u_0 \sim u^T \sim u u_0 I = ue^T + eu^T + u_0 I - 2u_0 ee^T$. (21) When $u \in Q$ is in the direct product of multiple second-order cones, the arrowhead matrix is formed by placing the appropriate matrices of the above form on the diagonal of the block. The arrowhead matrix has the property that, for any vector v , $Uv = u^T v$. Using this notation, Newton's equations in Eq. (20) can be written as $S X + S \bar{X} = \sigma\mu - \kappa \bar{\tau}$, (22) where X and \bar{X} are the arrowhead matrices for the vectors x and \bar{x} . Equations (19) and (22) together form Newton's system. We can see that there are $2N+K+3$ constraints to match the $2N+K+3$ variables in the vector $(x; y; \tau; \theta; s; \kappa)$. In reference [53], it is shown that, as long as the duality gap is positive and $(x; y; \tau; \theta; s; \kappa)$ is very far from the central path (which will be the case as long as σ is chosen close enough to 1 in each iteration), the Newton system has only one unique solution. Note that different search directions can be chosen than the one that arises when solving the Newton system presented here; this consists of first applying a scaling transformation to the product of second-order cones, then forming and solving the resulting Newton system, and finally applying the inverse scaling transformation. Alternative search directions are explained in Appendix D, but in the main text we stick to the basic search direction illustrated above, since in our numerical simulations the simple search direction gave equal or better results than more complex alternatives and enjoy of the same theoretical guarantee of convergence [53]. 5. Solve Newton's system Newton's system formed by combining the equations (19) and (22) is a linear $L \times L$ system of the form $Gu = h$, where $L = 2N+K+3$. Classically, this can be solved exactly in several ways, the simplest being Gaussian elimination, which scales as $O(L^3)$. Using Strassen-type tricks [54], this can easily and topically be sped up to $O(L\omega)$, where $\omega < 2.38$ [55], although in practice the execution time is closer to $O(L^3)$. , the linear system can be approximately solved using a variety of interactive solvers, such as conjugate gradient descent or the random Kaczmarz method [56]. The complexity of these approaches depends on the condition number of the Newton matrix. Section IV discusses quantum approaches to solving Newton's system. It is important to distinguish between methods that solve Newton's system exactly and methods that solve it inexactly, because inexact solutions generally lead to infeasible intermediate points.

VAR: where $\alpha \geq G$ is the normalization constant, chosen as $\alpha = GF$ for our use case. The other blocks in UG are irrelevant but must be encoded so that UG is unitary. For our purposes, we focus on real matrices G but the extension to complex matrices is straightforward. A block encoding uses unitary units that implement (controlled) state preparation as well as QRAM data structures to load classical data. Specifically, we refer to QRAM as the quantum circuit that allows query access to classical data in superposition, $\psi j |j\rangle |0\rangle \text{ QRAM} \rightarrow j \psi j |j\rangle |aj\rangle$

The idea is to choose the quantum algorithms of the circuits and perform larger calculations or build the algorithms within the curvatures of the black hole to build new horizons, new quantum sequences or quantum fields in 3 dimensions. New or spacecraft-like space stations that fit these terminal domains of a galaxy.

It would be better to test whether algorithms or whether quantum fields fit into the curved lines of the black hole to build space objects that function within a series of dimensions.

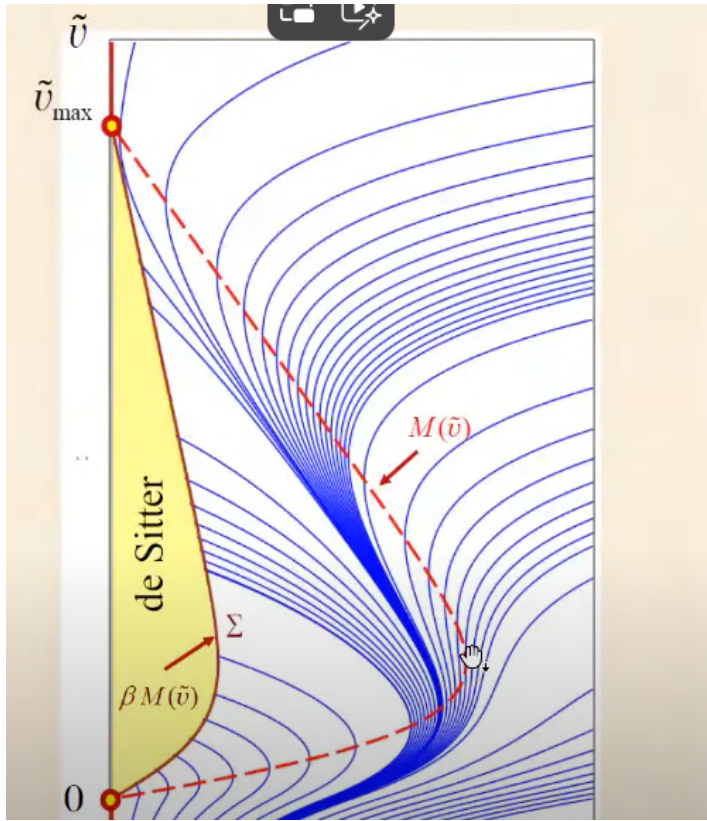
Image and Combination of QRAM within the Curvature of the Black Hole

The image is a Penrose diagram, which is a type of space-time diagram used in general relativity to represent the causal structure of space-time. The elements it shows are:

- **Axes and Labels:**
 - The vertical axis is labeled qq and pp at the top and bottom, respectively.
 - The horizontal axis is labeled $\pi/2$ and $-\pi/2$ on the left and right, respectively.
- **Regions:**
 - The upper region is labeled "infinite future tense."
 - The lower region is labeled "infinite past tense."
- **Curves:**
 - The black curves represent the boundaries of space-time.
 - The red dashed and solid curves represent surfaces of constant T , with $T=0$ and $T=\text{const}$ labeled.
 - The dashed red curve labeled Σ represents a specific surface in spacetime.

This diagram is interesting because it visually represents the causal structure of a space-time, showing how different regions and surfaces are connected. It is particularly useful in the study of black holes and cosmology, where understanding the causal relationships between different events is crucial.

Combining QRAM (Quantum Random Access Memory) within the curvature of a black hole and capturing signals with an FPGA or quantum chip using Qiskit Metal or Google Cirq is a fascinating idea. Capturing quantum signals in these environments could open new perspectives in quantum physics and the theory of quantum gravity.



Examples of the Image and Combination of QRAM within the Curvature of the Black Hole

The image is a diagram that appears to represent the causal structure of a space-time, possibly in the context of general relativity. The elements it shows are:

1. Axes and Labels:

- The vertical axis is labeled qq and pp at the top and bottom, respectively.
- The horizontal axis is labeled $\pi/2$ and $-\pi/2$ on the left and right, respectively.

2. Regions:

- The upper region is labeled "infinite future tense."
- The lower region is labeled "infinite past tense."

3. Curves:

- The black curves represent the boundaries of space-time.
- The red dashed and solid curves represent surfaces of constant $T=0$ and $T=const$ labeled.
- The dashed red curve labeled Σ represents a specific surface in spacetime.

This diagram is interesting because it visually represents the causal structure of a space-time, showing how different regions and surfaces are connected. It is particularly useful in the study of black holes and cosmology, where understanding the causal relationships between different events is crucial.

Combining QRAM in the Curvature of a Black Hole

Combining QRAM (Quantum Random Access Memory) within the curvature of a black hole and capturing signals with an FPGA or quantum chip using tools like Qiskit Metal or Google Cirq is a fascinating idea. This could open new perspectives in quantum physics and the theory of quantum gravity. Here are more examples related to these ideas:

Example 1: Quantum Data Capture in a Black Hole

Imagine a scenario in which an advanced quantum sensor is capable of operating near the curvature of a black hole. This sensor could capture quantum signals that not only describe the properties of the black hole, but also reveal information about additional dimensions or phenomena not directly observable from Earth. The integration of QRAM would allow these signals to be stored and processed efficiently, facilitating their subsequent analysis.

Example 2: Using FPGA for Real-Time Processing

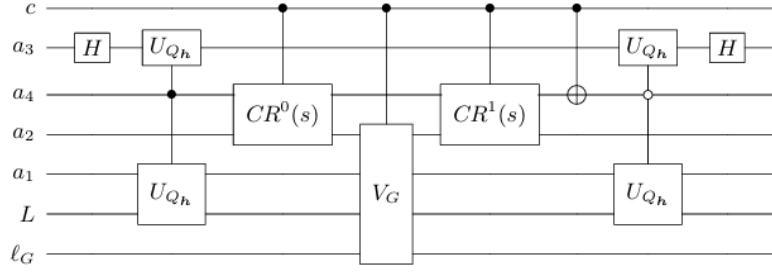
Using FPGA (Field-Programmable Gate Array) for real-time processing of quantum signals near a black hole could

Real-time processing of signals and images to build new spatial objects that fit two interesting concepts; Black holes and quantum circuits.

To build these objects or Domains we need to adapt space technology to the structures of black holes and ask ourselves where we will place the singularities offered by quantum circuits.

Quantum circuits: (1) Build circuits implementing unitary block coding UH and Uh up to error ϵG and ϵh using quantum state preparation and QRAM, which involves classical preprocessing cost scaling such as $L^2 \text{Polylog}(1/\epsilon G, h)$. The necessary quantum resources are described in Table III. T-gate count is $O(L^2)$. (2) Employ the unitary QLS S of Proposition 2 to approximately solve the corresponding QLSP, which leads to the quantum state $|\tilde{v}\rangle$. The complexity of the query to UG , er , its controlled versions and its inverses, is $O(\kappa F(G)\log(1/\epsilon))$. The number of qubits needed is $\log L + 5$. (3) Repeat the previous step $O(L\ln(L/\delta)\epsilon^{-2})$ many times to implement the pure-state quantum tomography scheme of section IV D, which also requires the use of an $O(L)$ qubit QRAM structure and a auxiliary qubit. The tomography leads to the classical vector estimation sought $\sim v$ with $\sim v - v \leq \epsilon$. The QLSS can then be used for the iteration of an IPM SOCP solver, which involves forming and solving a linear system of equations, which results in the QIPMSOCP solver. We provide the quantum circuits needed to implement the solver in Section IV F. However, we emphasize that we have not yet considered the various practicalities and difficulties of setting up a solver. end-to-end QIP SOCP solver, which is discussed later in Section V F. Quantum Circuits The following are the quantum circuits required for the QLSS of Proposition 1. The QLSS requires applying a unitary $U[s]$ for any different value of s , where $U[s]$ is a block encoding of some Hamiltonian related to G and h , as specified below. the L -labeled register-qubit and the G -labeled G -qubit register. These labels are used as subscripts in brackets, kets, and operators to clarify the register to which they apply. The circuit for $U[s]$ is shown in Fig. 1 and described in Ref. [18, Appendix E]. Specifically, the unitary $U[s]$ is a block encoding of the $(2+)$ -qubit Hamiltonian $c(s) \cdot H[s] := (1-f)$

$(s))H0+f(s)H1$ in the registers $sa4a1L$, where $c(s)$ is a normalization factor. [defined later in equation (60)], $H0 := \langle | \langle 0 0 IL - |h h|L 0 0 0 0 - IL IL - |h h|L 0 0 0 0 - IL 0 0 \rangle | \rangle$ (53) and $H1 := \langle | | \langle 0 0 0 G 0 0 G^\dagger (IL - |h h|L) 0 0 (IL - |h h|L)G 0 0 G^\dagger 0 0 0 \rangle | | \rangle$, (54) and where IL denotes the identity operation in subsystem L , and the four rows and columns correspond to the sectors with qubits $a4$ and $a1$ in $(0,0)$, $(0,1)$, $(1,0)$ and $(1,1)$. Figure 1 presents the expressions $CR0(s) := |0 0|a4 \otimes R(s)a2 + |1 1|a4 \otimes Ha2$, (55) $CR1(s) := |1 1|a4 \otimes R(s)a2 + |0 0|a4 \otimes Ha2$, (56) $VG := |0 0|a2 \otimes Za1 \otimes ILG + |1 1|a2 \otimes 0 UG U^\dagger G 0 a1LG$



The controlled version of the quantum circuit in Fig. 1, controlled on qubit c . Note that not all gates need to be controlled on their inverses follow in the circuit.

The idea is to create a ship where quantum algorithms and the structures of black holes fit together to generate advances in space technology and quantum technology and combine them together to trace routes that take us to the future where ships can be made to navigate well in the harshest conditions. space conditions with emerging quantum technologies as if the spacecraft were itself a quantum object within an emulated or virtual quantum field of curves and tensors of the black hole at a structural level.

A spaceship built with quantum technologies that is capable of crossing galaxies by thinking and building quantum technologies and hard razr FPGAs that are more resistant to low temperatures.

Example 1: Quantum Data Capture in a Black Hole

Imagine a scenario in which an advanced quantum sensor is capable of operating near the curvature of a black hole. This sensor could capture quantum signals that not only describe the properties of the black hole, but also reveal information about additional dimensions or phenomena not directly observable from Earth. The integration of QRAM would allow these signals to be stored and processed efficiently, facilitating their subsequent analysis.

Example 2: Using FPGA for Real-Time Processing

Using FPGA (Field-Programmable Gate Array) for real-time processing of quantum signals near a black hole could enable real-time data capture and analysis. This would open the possibility of building new space objects that integrate concepts of black holes and quantum circuits.

To build these objects or domains, we need to adapt space technology to the structures of black holes and consider where to place the singularities offered by quantum circuits.

Quantum Circuits:

1. **Circuit Construction:** Build circuits implementing unitary block coding $U_{H,U}$ and $U_{h,U}$ up to error $\epsilon_G \backslash epsilon_G$ and $\epsilon_h \backslash epsilon_h$ using quantum state preparation and QRAM, which involves classical preprocessing cost scaling such as $L^2 \log(1/\epsilon_G, h) L^2 \backslash log(1 \backslash epsilon_{\{G,h\}})$. The necessary quantum resources are described in Table III. The gate count T is $O(L^2)O(L^2)$.
2. **Using the QLS:** Use the unitary $ULSU_{\{LS\}}$ of Proposition 2 to approximately solve the corresponding QLSP, leading to the quantum state $|v \sim \tilde{v}\rangle$. The complexity of the query to $UGU_G, \epsilon_h \backslash epsilon_h$, its controlled versions and its inverses, is $O(\kappa F(G) \log(1/\epsilon) O(\kappaappa F(G) \log(1 \backslash epsilon))$. The number of qubits needed is $\log L + 5 \log L + 5$.
3. **Implementation of Quantum Tomography:** Repeat the above step $O(L \ln(L/\delta) \epsilon^{-2}) O(L \ln(L/\delta) \epsilon^{-2})$ many times to implement the pure-state quantum tomography scheme. This requires the use of an $O(L)O(L)$ qubit QRAM structure and an auxiliary qubit. The tomography leads to the classical vector estimation sought $\vec{v} \backslash vec\{v\}$ with $\|\vec{v} - v\| \leq \epsilon \|\vec{v}\|$.

Quantum Spaceship

The idea is to create a ship where quantum algorithms and black hole structures fit together to generate advances in space technology and quantum technology. By combining them, we could chart routes that take us into the future, allowing ships to navigate well in the harsh conditions of space with emerging quantum technologies. Imagine a spacecraft that is itself a quantum object within a virtual quantum field, emulated by the curves and tensors of the black hole at a structural level.

A spacecraft built with quantum technologies would be able to traverse galaxies using quantum technologies and FPGAs that are more resistant to low temperatures. This would open new opportunities for space exploration and understanding quantum phenomena in the universe.